doi.org/10.1002/batt.202000046

Hierarchically Porous Biomass Carbon Derived from Natural Withered Rose Flowers as High-Performance Material for Advanced Supercapacitors

Abrar Khan,[a] Raja Arumugam Senthil,[a] Junqing Pan,*[a] Yanzhi Sun,[a] and Xiaoguang Liu[a]

Herein, a hierarchically porous carbon was derived from the natural withered rose flower (denoted as RDPC) through a facile two-step method of carbonization and chemical activation with a mixture of KOH/KNO_3. The as-derived RDPC contains an enlarged specific surface area of 1980 $m^2 g^{-1}$, better electrical conductivity and hierarchical porous architectures. Under three-electrode system with 6 M KOH electrolyte, the RDPC displays a wonderful electrochemical activity as supercapacitor electrode including of ultrahigh SC (350 $F g^{-1}$ at 1 $A g^{-1}$), superb rate ability (165 $F g^{-1}$ even at 150 $A g^{-1}$) and remarkable durability (only 4.4% fading rate of capacitance after 140,000 cycles at 100 $A g^{-1}$). The RDPC based symmetric supercapacitor with 6 M KOH electrolyte supplies the highest energy density of 15.6 $Wh kg^{-1}$ at 499 $W kg^{-1}$ with only 3.5% decay rate of capacitance over 15,000 cycles at 20 $A g^{-1}$, which is revealing the excellent real application of RDPC in the supercapacitor. This extraordinary electrochemical performance of RDPC can be attributed to its uniform interconnected layered-like morphology, hierarchical porous networks, large specific surface area and fast electrochemical kinetics. Therefore, it is indicating that a facile and inexpensive designing of porous carbon from naturally available withered rose flowers and is a more sustainable electrode material for advanced energy storage related applications.

1. Introduction

Due to the worldwide energy shortages and environmental problems by continuous production of the traditional fossil fuels, it is an urgent task to develop and establish green, inexpensive and sustainable energy storage technologies.[1,2] Supercapacitors have the outstanding properties of quick charge-discharge rate, huge power density, low-cost and long cycle life which have been extensively acknowledged as an advanced green energy storage technology.[3–5] Recently, supercapacitors have been widely used in daily life, like portable devices hybrid electric vehicles. Alternatively, the lower energy density of supercapacitors is seriously restricted their large-scale applications and as independent power for all-electric cars. The energy storage abilities of supercapacitors are fundamentally based on their active electrode materials. Consequently, the development of higher efficient and low-cost active electrode material played key roles for the improvement of supercapacitors.

There are three types of active materials which have mostly utilized as electrode material for supercapacitors, like metal oxides,[6–8] polymers[9–11] and derived carbons.[12–15] Due to the distinct pseudocapacitive properties, the conducting polymers and metal oxides offered a high specific capacitance (SC) for supercapacitors. Nevertheless, the relatively low conductivity, power density and short-term cyclic life with higher cost as their shortcomings limited the real application.[16] Meanwhile, the conducting polymers are also facing some problems like loss of capacitive performance quickly due to the deformation effects of the electrode material during the charge/discharge processes.[17] Among these materials, the carbon has a unique property of large specific surface area (SSA), abundant active sites with outstanding chemical stability, leading to favorable electrochemical properties.[18,19] Recently, the activated carbon, namely porous carbon (PC) has been received focused attention as electrode material for supercapacitors as a result of its remarkable SSA, well-arranged porous structure and very long-cyclic stability. The PC can be synthesized from various precursors, mainly biomass wastes, polymers and metal organic frameworks (MOFs). It is noticed that the high cost of ligand, low yield and the pollution of nitrate wastewater largely reduced their large-scale applications of polymers and MOFs.[20–24]

Compared with these two precursors, the waste biomass are a readily available, low-cost, environmental-friendly to produce natural PC material.[25,26] The naturally available waste biomass are substantially contains the three components of cellulose, hemicelluloses, and lignin.[27–29] Mostly, the PCs derived from biomass wastes through carbonization and chemical activation treatments in inert condition.[30,31] The biomass wastes converted into biochar after the carbonization treatment. Subsequently, the resultant biochar is activated with activators such as $ZnCl_2$, KOH, NaOH, Na_2CO_3, $MgCO_3$ and $CuCO_3$ resulting to increased SSA, rich porosity and related high SC.[32–37]

[a] A. Khan, Dr. R. Arumugam Senthil, Prof. J. Pan, Prof. Y. Sun, Prof. X. Liu
State Key Laboratory of Chemical Resources Engineering
Beijing Advanced Innovation Center for Soft Matter Science and Engineering
College of Chemistry,
Beijing University of Chemical Technology,
Beijing 100029, P.R. China
E-mail: jqpan@mail.buct.edu.cn

Supporting information for this article is available on the WWW under https://doi.org/10.1002/batt.202000046

Up to date, the different kinds of biomass wastes have been extensively utilized to prepare PCs with high SC for supercapacitors.[38–43] For example, Gong and his coworkers reported the biomass derived PC from bamboo with an SC of 171 $F g^{-1}$ at 1 $A g^{-1}$. This PC based symmetric supercapacitor showed a good cyclic performance and kept 84% of SC after 5,000 cycles at 1 $A g^{-1}$.[44] Liu et al. reported the PC from Jujun grass, which can provide a huge SC of 296 $F g^{-1}$ at 1 $A g^{-1}$ with 87.3% of SC retention over 2,000 cycles.[45] Xie et al. reported the PC derived from camellia oleifera shell for supercapacitors, which supplied a high SC of 315 $F g^{-1}$ at 0.5 $A g^{-1}$ with keeps 90% of SC over 5,000 cycles at 10 $A g^{-1}$ in 2 M H_2SO_4 electrolyte. As well, this PC delivered a SC of 251 $F g^{-1}$ at 0.5 $A g^{-1}$ with 89% of SC retention over 5000 cycles even at 20 $A g^{-1}$ in 6 M KOH electrolyte.[46] More recently, Xe et al. designed the PC from camellia oleifera via microwave treatment with a maximum SC of 367 $F g^{-1}$ at 0.5 $A g^{-1}$ with holding 99% of SC after 10,000 cycles at 10 $A g^{-1}$ in 2 M H_2SO_4 electrolyte.[47] Up to now, the large-scale application of biomass PCs has still limited by their low SC and energy density. Hence, it is very essential to exploit a more suitable biomass precursor to obtain high efficient PC from the diversity of nature. Flowers, especially the roses are one of the most popular flowers in the world, and a large number of waste withered roses have been disposed every day. However, only a few papers have pay attention to develop the biomass PC from the withered flowers and used as electrode material for supercapacitors.[48–51]

Herein, we have proposed and derived an interconnected layered-like hierarchical PC with high-performance from withered rose flower wastes in first time by two steps of carbonization and combined KOH/KNO_3 activation processes. Due to used mixture of KOH/KNO_3 for activation, the resultant rose flower derived PC (RDPC) contains an enlarged SSA of 1,980 $m^2 g^{-1}$ and well-organized porosity. The electrochemical results indicate that the as-prepared RDPC electrode exhibits a great SC of 350 $F g^{-1}$ at 1 $A g^{-1}$ and amazing cyclic stability with high retention rate of 95.6% of SC after 140,000 cycles at 100 $A g^{-1}$ in a three-electrode setup in 6 M KOH electrolyte. Besides, the RDPC based symmetric supercapacitor provides wide operating potential (1.5 V) and high energy density 15.6 $Wh kg^{-1}$ at 499 $W kg^{-1}$ in 6 M KOH electrolyte. Consequently, this work provides a low-cost and sustainable method for the satisfactory employment of waste biomass to prepare highly efficient PC material for supercapacitors.

2. Results and Discussion

2.1. Morphological and Structural Analysis

The detailed preparation route of RDPC from withered rose flowers are schematically displayed in Figure 1. It is displayed that RDPC derived from withered rose flowers via a two-step method of carbonization and chemical activation with the using of KOH/KNO_3 mixture as the activator. Firstly, the dried rose flowers were converted into biochars via a simple carbonization treatment. After that, the attained biochars were

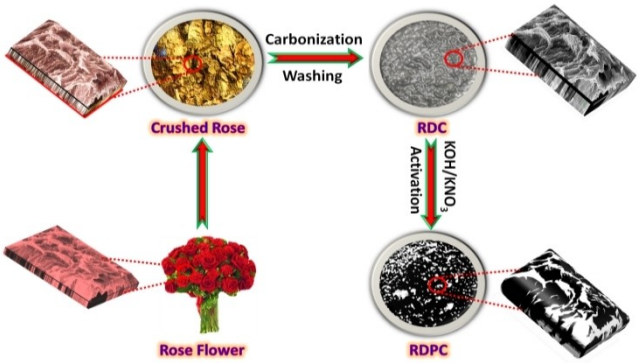

Figure 1. Schematic diagram for the preparation of RDPC from the withered rose flower by combined carbonization and KOH/KNO_3 activation processes.

activated with the mixture of KOH/KNO_3 under N_2 atmosphere, yielding to format well-organized hierarchical porous structures via the release of gases byproducts. The formative porous structure is more beneficial to enlarge its SSA, which will be helpful for the raising of its electrochemical activity for supercapacitors.[31,52]

The SEM measurement was employed to explore the surface-structure of RDC and RDPC samples, and the observed SEM images at various magnifications are displayed in Figure 2 (a–f). Figure 2(a–c) showed the morphology of RDC which exhibits an interconnected layered-like structure. And Figure 2 (d–f) showed the morphology of RDPC, the attained RDPC still keep its similar interconnected layered-like structure after activation process. We also observed that the appearance of corrosion on the RDPC surface indicates the porosity on the carbon surface by the released pyrolysis gas during activation treatment. The detailed information about these microstruc-

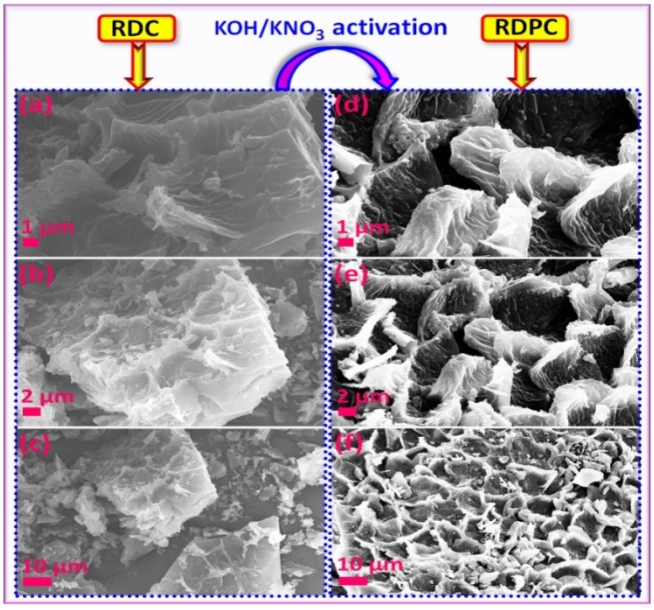

Figure 2. SEM images of the obtained a-c) RDC and d-f) RDPC samples under various magnifications.

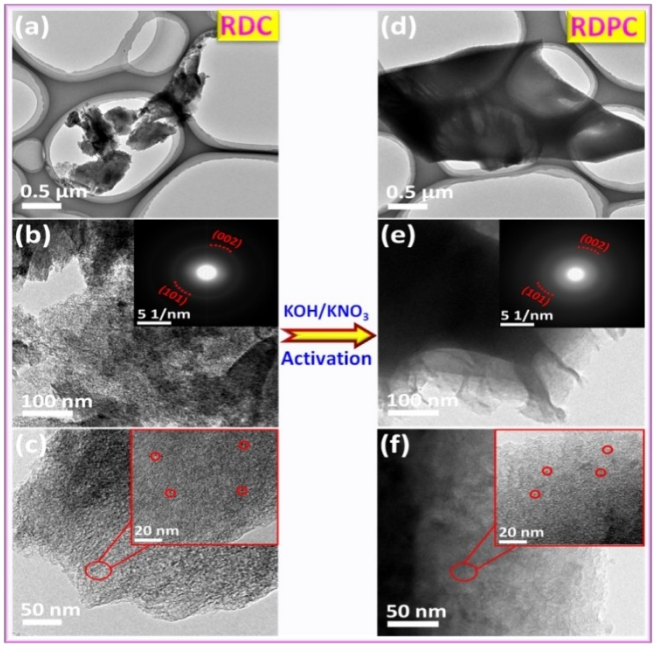

Figure 3. Different resolution HR-TEM images and SAED patterns of the obtained a-c) RDC and d-f) RDPC samples.

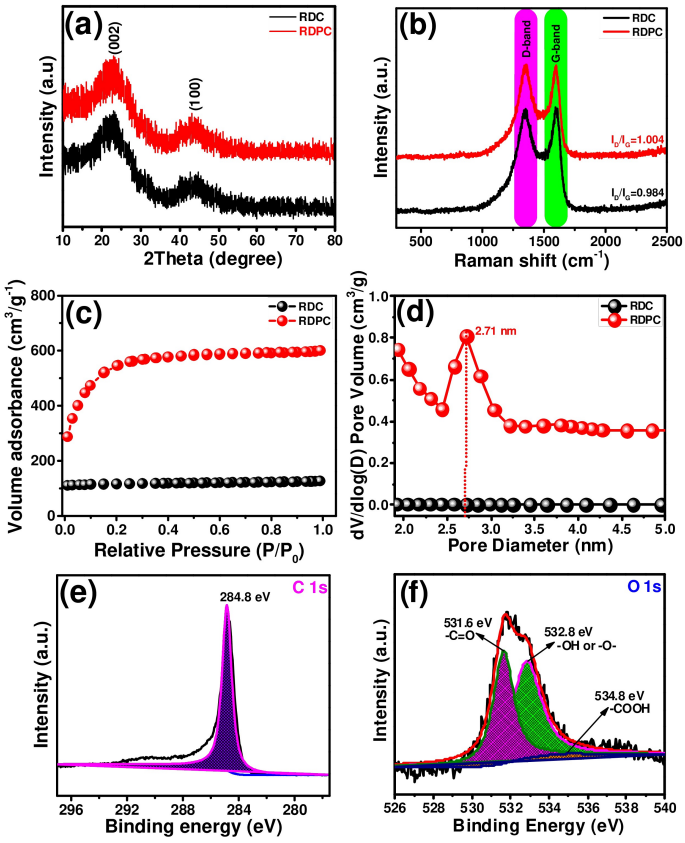

Figure 4. a) XRD patterns, b) Raman spectra, c) nitrogen adsorption-desorption isotherms and d) pore-size distributions of the obtained RDC and RDPC samples; e,f) high resolution XPS spectra of RDPC sample: e) C 1s and f) O 1s.

tures and porosities are analyzed by the HR-TEM test. The HR-TEM images and SEAD pattern of RDC and RDPC samples are displayed in Figure 3(a–f). As depicted in Figure 3(a–c), the RDC possesses a layered-stacking structure. The RDPC possesses a similarly layered-stacking structure with the occurrence of well-organized meso-pores on the carbon frameworks in Figure 3(d–f). The occurrence of meso-pores is helpful to reduce the ion diffusion length and improve more accessibility of the electrolyte ions on the RDPC, leading to the greatly enhanced electrochemical performance.[53,54] As seen from SAED patterns, the detected two cycles belong to (002) and (101) crystalline planes of two samples, demonstrating the successful preparation of RDPC from almost freely available withered rose flowers.

XRD and Raman spectroscopy analyses were employed to further investigate the phase purities and microstructures of the carbon samples. The resultant XRD patterns of RDC and RDPC samples are illustrated in Figure 4(a). As seen from Figure 4(a), only two expanded XRD peaks are detected for both of RDC and RDPC samples at 22.5° and 43.7°, which belong to their (002) and (100) diffraction planes, respectively (PDF#41-1487).[21,52] The XRD results further expressed the successful preparation of carbon material from withered rose flowers with high purities. Besides, the peak intensities of RDPC are slightly higher than those of RDC, implying the slight increases of the graphitization degree of carbon after KOH/KNO_3 activation treatment under high temperature. The Raman spectra of RDC and RDPC samples are showed in Figure 4(b). It demonstrates that only two distinctive peaks are observable in both of RDC and RDPC at 1,354 and 1,597 cm^{-1}, belonging to D-band and G-band of disordered carbon and graphitic phase carbon, respectively.[41] The peak intensity ratios of ID/IG are determined as 0.984 and 1.004, respectively. The RDPC shows a slightly higher I_D/I_G ratio, suggesting the slightly increased graphitization degree of RDPC during the KOH/KNO_3 activation under high temperature. It is beneficial to improve the electrochemical ability of RDPC, including its electric conductivity and rate performance. These observed Raman spectroscopy results are well coincided with the HR-TEM and XRD analyses.

For the further evaluation the change of SSA and porosity of carbon before and after combined KOH/KNO_3 activation treatment, Figure 4(c) illustrates the N_2 adsorption/desorption isotherms of RDC and RDPC samples. As showed in Figure 4(c), the RDC shows a type-II isotherm, suggesting the carbon has a nonporous surface before the activation process. In the meantime, the RDPC has a typical type-I and type-IV isotherms with a large quantity of N_2 absorbability, demonstrating the existence of rich micro-pores and meso-pores on the RDPC surface after activation.[55,56] These well-organized porous structures has more favorable electrochemical active sites and less-resistance channels for the fast-diffusion of electrolyte and ions, leading to increased SC and rate performance.[57–59] We also observed that the SSA of RDC and RDPC are 1,203 and 1,980 m^2g^{-1}, respectively. It clearly indicates the great enlargement in the SSA of carbon after activation under the optimized condition. According to the BJH model, the pore size distribution of the RDC and RDPC are represented in Figure 4(d). There is no peak appeared in the RDC indicates that its nonporous character-

istics. However the RDPC contains peaks about below 2 nm and 2.71 nm, proving the availability of interconnected micro-pore and meso-pore sized porosity on the surface of RDPC frameworks. The achieved micro/meso-pores structures have more advantages to increase the SC and rate ability.[33,34]

The XPS spectra of as-prepared RDPC are presented in Figure S1 and Figure 4(e,f). As seen in Figure S1, the full survey XPS spectrum only shows a strong intense peak of C element and a low intense peak of O element, representing the high purity of the as-prepared RDPC sample. The high-resolution of C 1s spectrum in Figure 4(e) contains a peak at 284.8 eV, which belongs to the C=C bond of graphitic carbon.[44,52] And the high-resolution of O 1s spectrum (Figure 4(f)) exhibits a three peaks at 531.6, 532.8 and 534.8 eV which are referred to the C=O, –OH or –O– and –COOH bonds, respectively.[46,47] The above characterization results demonstrate that the withered rose flowers are a potential raw material to prepare high purity biomass carbon with well-arranged porous structures.

2.2. Electrochemical Ability in Three-Electrode System

The supercapacitive performances of as-derived biomass carbon materials were tested via CV and GCD measurements by three-electrode in 6 M KOH electrolyte. In order to prepare a high SC electrode material, the influences of KOH/KNO_3 weight ratios, activation temperatures and activation times on the effect of RDPC were systematically studied at 1 A g^{-1}, and the results are presented in Figure S2, Figure S3(a,b) and Figure S4 (a,b), respectively. As seen from Figure S2, the RDC activated with mixture of KOH/KNO_3 in a weight ratio of 100:100:0.5 has a superior electrochemical performance than those with individual KOH and KNO_3. Overall, the optimization experiments indicate that the optimal conditions for the preparation of highest performance RDPC are as followed: RDC:KOH:KNO_3 = 100:100:0.5 at 700 °C for 2 h. Figure S5(a) illustrates the CV curves of RDC and RDPC electrodes at a scan rate of 1 mV s^{-1}. The CV curves show typical rectangular shapes, meaning the electrical double-layer capacitance (EDLC) processes.[60,61] The RDPC electrode exhibits much larger CV curve area than that of the RDC electrode, demonstrating greatly enhanced electrochemical performance of RDPC electrode after KOH/KNO_3 activation. The outstanding electrochemical performance of RDPC electrode was also confirmed by GCD tests at 1 A g^{-1}, and the results as shown in Figure S5(b). The RDPC electrode supplies an SC of 350 F g^{-1}, which is much greater than the RDC electrode (231 F g^{-1}). Thereafter, the Nyquist plots of RDC and RDPC electrodes are given in Figure S5(c). The results exhibited that RDPC electrode has higher electrical conductivity and EDLC behavior. On the other hand, the combined activation of KOH/KNO_3 can be creating micro and meso porous structure on the surface of RDPC, which is helpful to enlarge its SSA, resulting in the increased SC as electrode material for supercapacitors.

In addition, the CV curves for the optimized RDPC electrode at various scan rates (1 to 600 mV s^{-1}) are displayed in Figure 5 (a). All of these CV curves have a uniform rectangular structure,

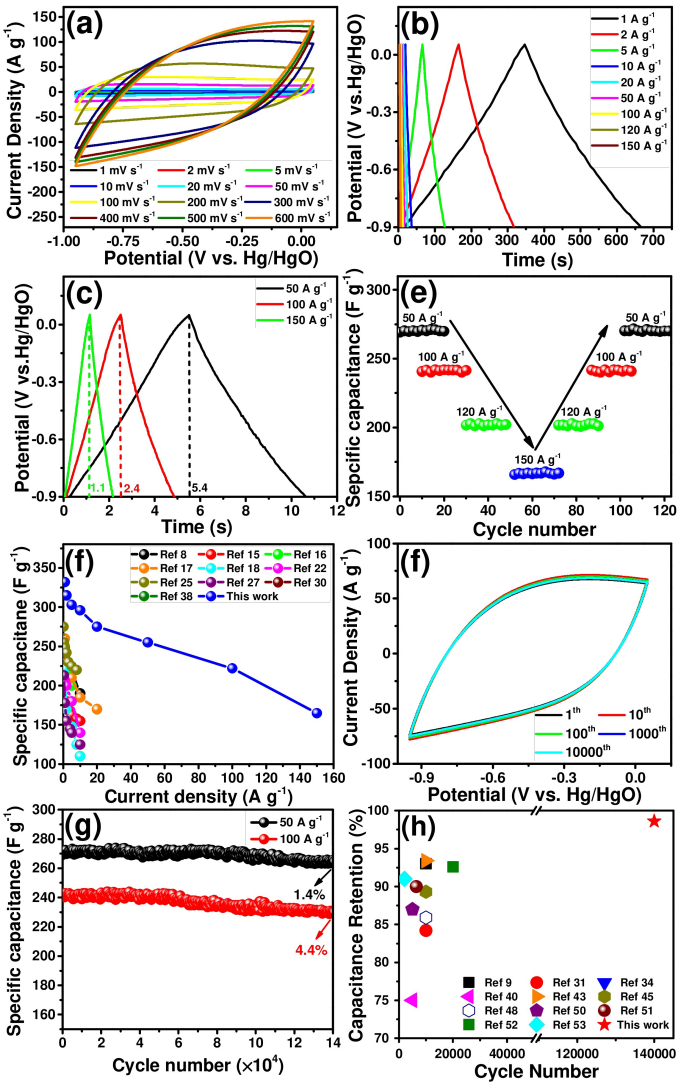

Figure 5. Electrochemical properties of RDPC by three-electrode system in 6 M KOH electrolyte: a) CV curves at various scan rates (1–600 mV s^{-1}), b) GCD curves at various current densities (1–150 A g^{-1}), c) Details GCD curves at high current densities of 50, 100 and 150 A g^{-1}, d) Plots of SC versus cyclic number at various current densities, e) Comparison of SC of RDPC and the other reported biomass carbons under various loads, f) CV curves at super-fast sweep speed of 200 mV s^{-1} for 10,000 cycles, g) Long-cyclic durability tests of 140,000 GCD cycles at ultra-high current densities of 50 and 100 A g^{-1}, and h) Comparison of cyclic durability of the RDPC and the other reported carbon materials in the literature.

representing the excellent reversibility and fast electrochemical kinetics of the RDPC electrode. Figure 5(b,c) show the GCD plots of the RDPC electrodes at various current densities (1 to 150 A g^{-1}). It is found that the RDPC electrode maintains a typical triangular shape GCD plot even at 150 A g^{-1}, which is evidence for the wonderful capacitive property and excellent reversibility. The observed GCD results are well matched with the CV tests. In other hand, the RDPC electrode supplies a high SC of 350 F g^{-1} at 1 A g^{-1} and 165 F g^{-1} at 150 A g^{-1}, revealing its remarkable capacitive and rate ability. Apart from that, the charge/discharge time of RDPC electrodes are greatly reduced to 5.4, 2.4 and 1.1 s at super-high current densities of 50, 100 and 150 A g^{-1}, as shown in Figure 5(c). This outstanding electro-

chemical performance is mainly beneficial from its large SSA, hierarchical porous and special interconnected layered-like structures.[60–62] The plots of SC versus cyclic numbers at various current densities (50 to 150 A g^{-1}) are presented in Figure 5(d). This test is further proved the attractive rate and reversibility of RDPC electrode. Figure 5(e) displays the comparison of SC of RDPC electrode with other reported biomass carbons at various current densities. As seen from Figure 5(e), the RDPC electrode show much high SC and rate performance than those of previously reported carbon electrodes.[8,15–18,22,25,27,30,38] The long-term stability of the RDPC electrode was investigated by CV and GCD tests, and the results are shown in Figure 5(f) and Figure 5(g). It can be observed that all of these CV curves nearly overlapped each other, indicating its remarkable cyclic stability. Similarly, the RDPC electrode possesses remarkable cyclic stability with very high SC retention of 98.6 and 95.6% for extra-long 140,000 cycles at 50 and 100 A g^{-1}, respectively. The RDPC electrode also shows the superior SC retention than that of previously reported carbon electrodes in the literature, as shown in Figure 5(h).[9,31,34,40,43,45,48,50–53] The attained excellent cyclic stability of RDPC may be attributed from its superb interconnected layered structure, large SSA and high porosity with micro and meso porous networks. As well, this result is suggested that the as-prepared RDPC material has great potential for large-scale application in the supercapacitors.

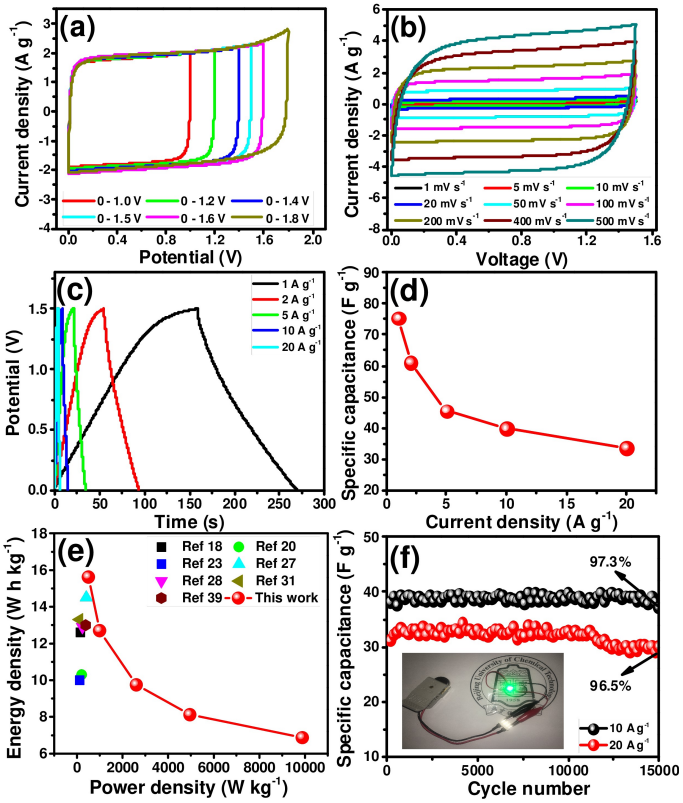

Figure 6. Electrochemical properties of RDPC based symmetric supercapacitor in 6 M KOH aqueous electrolyte: a) CV curves in the different potential windows at a scan speed of 200 mV s^{-1}, b) CV curves in the potential window of optimal voltage of 1.5 V at various scan rates (1-500 mV s^{-1}), c) GCD curves at various current densities (1–20 A g^{-1}) in the potential window of 1.5 V, d) observed SC at various current densities, e) Comparison of Ragone plots of RDPC and the other reported biomass carbons in the literature, and f) Cycling durabilities for 15,000 GCD cycles at 10 and 20 A g^{-1} (Inserted: a red LED light powered by the assembled symmetric supercapacitor).

2.3. Electrochemical Properties of Symmetric Supercapacitor

To further confirm the real application of RDPC material, the coin-cell like symmetric supercapacitor (SSC) was assembled with RDPC electrodes in 6 KOH as electrolyte. Figure 6(a) illustrates the CV curves of as-assembled SSC operated in various potential windows at 200 mV s^{-1}. It is noticed that the SSC can work in a broad applied potential ranges from 0 to 1.5 V. The slightly increased working voltage of assembled SSC of 1.5 V may be beneficial from the highly ordered RDPC with the new created micro and meso porous structures, which is helpful to reduce the ion diffusion length and improve more accessibility of the electrolyte ions on the RDPC. Afterwards, the CV curves of SSC in a potential window of 1.5 V at various scan rates from 1 to 500 mV s^{-1} are illustrated in Figure 6(b). The rectangular shape CV curves were found to retain even at 500 mV s^{-1}, meaning its EDLC behavior with excellent rate performance. Figure 6(c) illustrates the GCD plots of SSC at various current densities (1 to 20 A g^{-1}). It is found that all plots kept their typical triangular shapes, illustrating the outstanding rate performances.[30,63–65] The SC of these SSCs is presented in Figure 6(d). It can be seen that SSC offers high SCs of 75.3, 61.1, 45.6, 39.8 and 33.7 F g^{-1} at 1, 2 5, 10 and 20 A g^{-1}, respectively.

The Ragone plot of assembled SSC was compared with some of the published carbon electrodes in Figure 6(e). As shown in Figure 6(e), the assembled SSC offered the energy densities of 15.62 and 6.87 Wh kg^{-1} at 499 and 9892 W kg^{-1}, respectively. It is much greater than those published carbon electrodes.[18,20,23,27,28,31,39] Furthermore, the cycling stability of the assembled SSC at 10 and 20 A g^{-1} are shown in Figure 6(f). The assembled SSC displays the outstanding cyclic stability with retention rates of 97.3 and 96.5% of its initial SC after 15,000 GCD cycles at 10 and 20 A g^{-1}, respectively. Finally, Figure 6(f) exhibits the green light-emitting-diode (LED) lamp was powered by as-assembled SSC, which is a witness of real-life application of the RDPC electrode. The work indicates that withered rose flowers derived RDPC is a promising candidate as the sustainable electrode for high-performance energy storage devices.

3. Conclusions

In conclusion, we reported an efficient and cost-effective approach to prepare an interconnected layered-like RDPC material successfully from the natural rose flower as a sustainable and earth-abundant carbon precursor via the combined carbonization and KOH/KNO_3 activation for supercapacitor application. The obtained RDPC exhibits a high SSA of 1,980 m^2 g^{-1} and well-developed porous architecture. Based on these remarkable properties, the RDPC electrode offers a great SC (350 F g^{-1} at 1 A g^{-1}), superb long-cyclic life (4.4% of

SC decay rate after 140,000 cycles at 100 $A g^{-1}$) and excellent rate capability (165 $F g^{-1}$ at 150 $A g^{-1}$) by three-electrode in 6 M KOH electrolyte. Furthermore, the RDPC electrode offered a prominent energy density of 15.6 $Wh kg^{-1}$ at 499 $W kg^{-1}$ with maintained 96.5% of SC over 15,000 cycles at 20 $A g^{-1}$ for the RDPC based cell in 6 M KOH electrolyte. As a result, the green, cost-effective and renewable preparation of RDPC from the natural rose flower will be a talented material for the manufacture of advanced supercapacitors.

Experimental Section

Chemical and reagents

Absolute ethanol (99.7%), sodium hydroxide (NaOH, 99%) and hydrochloric acid (HCl, 36–38%) and potassium nitrate (KNO3, 99.8%) were supplied by Beijing Chemical Works, China. Polytetrafluoro ethylene (PTFE, 60%) was ordered from Shanghai Microtechnology Co. Limited, China. Potassium hydroxide (KOH, 98%) was purchased from Beijing Huarong Chemical Factory, China.

Porous carbon derived from natural withered rose flowers

In this section, 4 g dried rose flowers were well crushed by crusher, followed by washed with deionized (DI) water and ethanol to eliminate the surface impurities. It was put in over for drying at 80 °C for 4 h. The dried rose flowers were carbonized at 700 °C for 1.5 h in a nitrogenous atmosphere. After carbonization, the black-colored product was washed by 1 M HCl and DI water to remove the remained impurities and then dried at 80 °C for 4 h. The derived carbon of this step was denoted as RDC. After that, the RDC sample was well mixed with KNO_3 and KOH in a weight ratio of 100:0.5:100 and activated at 700 °C for 2 h in nitrogenous atmosphere. Then the collected product was washed by 1 M HCl and DI water until the pH of the filtrate was neutral and put in the oven for drying at 80 °C for 4 h. The finally derived PC was denoted as RDPC.

Physical characterizations

A sequence of characterization techniques including SEM, HR-TEM, XRD, Ramanspectroscopy, XPS and BET have been performed for the as-derived carbon samples for the examination of their microstructures, phase purity, SSA and chemical compositions. The details of the mentioned characterization instruments are displayed in Table S1.

Fabrication of working electrode

For the working electrode, 4:1:1 mass ratio of biomass carbon (200 mg), expanded graphite (50 mg), and 60 wt% PTFE solution (50 mg)were grounded uniformly via a mortar and pestle. Subsequently, it was rolled into a thin electrode membrane (50 μm thickness) via a roller machine. Afterwards, the carbon thin membrane was cut into pieces with the size of 10×10 mm^2 (mass loading active carbon about 2 $mg cm^{-2}$). The piece was pressed onto the same size Ni foam and followed by spot welded with Ni wire to attain a carbon working electrode.

Electrochemical measurements

A typical electrochemical test, the carbon based electrode carried as working electrode with Ni plate auxiliary electrode (1×1 cm^2), Hg/HgO reference electrode and 6 M KOH electrolyte to form three-electrode system to investigate its electrochemical performance. A LANHE battery station (CT3001A, Wuhan, China) was employed to carry out the galvanostatic charge-discharge (GCD) tests. Meanwhile, a CHI electrochemical workstation (CHI760D, Shanghai, China) was used to perform the cyclic voltammetry (CV) measurement. In the three-electrode system, the SC of carbon electrode material was determined from the discharging portion of GCD profile based on the following Equation (1) [30,48],

$$C_s = I \times \Delta t / (\Delta V \times m) \quad (1)$$

Where, C_s represents the SC of active material ($F g^{-1}$), I refer to the discharge current (A), Δt related to the discharge time (s), I corresponds to the mass of the active material, and ΔV indicates the potential window after the *IR* drop (V).

Afterwards, two identical RDPC electrodes based coin-like supercapacitor (SSC) was assembled in 6 M KOH electrolyte to prove the industrial usage. The energy and power densities of SSC was determined via GCD profiles from the following Equations (2,3) [31,33],

$$E = C_t (\Delta V)^2 / (2 \times 3.6) \quad (2)$$

$$P = 3600 \times E / t \quad (3)$$

Where, C_t, P and E refer to the SC ($F g^{-1}$), energy density ($Wh kg^{-1}$), and power density ($W kg^{-1}$) of the as-constructed SSC, respectively..

Acknowledgements

This work was supported by the by the National Key Research and Development Program of China (Grant No. 2019YFC1908304), National Natural Science Foundation of China (21676022 & 21706004) and the Fundamental Research Funds for the Central Universities (BHYC1701A).

Conflict of Interest

The authors declare no conflict of interest.

Keywords: biomass · hierarchical porous carbon · cost effectiveness · electrode material · supercapacitors

[1] J. Qi, X. Lai, J. Wang, H. Tang, H. Ren, Y. Yang, Q. Jin, L. Zhang, R. Yu, G. Ma, *Chem. Soc. Rev.* **2015**, *44*, 6749–6773.
[2] H. Laura, V. Marcio, P. Anisha, N. Mark, U. Patrick, M. Julie, *J. Phys. Chem. C* **2010**, *115*,1649–1658.
[3] A. Borenstein, O. Hanna, R. Attias, S. Luski, T. Brousse, D. Aurbach, *J. Mater. Chem. A* **2017**, *5*, 12653–12672.
[4] C. Qu, Y. Jiao, B. Zhao, D. Chen, R. Zou, K. S. Walton, M. Liu, *Nano Energy* **2016**, *26*, 66–73.
[5] Q. Zhang, E. Uchaker, S. L. Candelaria, G. Cao, *Chem. Soc. Rev.* **2013**, *42*, 3127–3171.
[6] G. Wang, L. Zhang, J. Zhang, *Chem. Soc. Rev.* **2012**, *41*, 797–828.

[7] W. Wei, X. Cui, W. Chen, D. G. Ivey, *Chem. Soc. Rev.* **2011**, *40*, 1697–1721.
[8] S. Faraji, F. N. Ani, *J. Power Sources* **2014**, *263*, 338–360.
[9] H. Gao, K. Lian, *RSC Adv.* **2014**, *4*, 33091–33113.
[10] J. Chen, C. Du, Y. Zhang, W. Wei, L. Wan, M. Xie, Z. Tian, *Polymer* **2019**, *162*, 43–49.
[11] M. E. Holtz, Y. Yu, D. Gunceler, J. Gao, R. Sundararaman, K. A. Schwarz, T. A. Arias, H. D. Abruña, D. A. Muller, *Nano Lett.* **2014**, *14*, 1453–1459.
[12] F. Beguin, V. Presser, A. Balducci, E. Frackowiak, *Adv. Mater.* **2014**, *26*, 2219–2251.
[13] H. Jiang, P. S. Lee, C. Li, *Energy Environ. Sci.* **2013**, *6*, 41–53.
[14] L. L. Zhang, X. Zhao, *Chem. Soc. Rev.* **2009**, *38*, 2520–2531.
[15] W. J. Lu, S.-Z. Huang, L. Miao, M.-X. Liu, D.-Z. Zhu, L.-C. Li, H. Duan, Z.-J. Xu, L.-H. Gan, *Chin. Chem. Lett.* **2017**, *28*, 1324–1329.
[16] M. Zhi, C. Xiang, J. Li, M. Li, N. Wu, *Nanoscale* **2013**, *5*, 72–88.
[17] L. Nyholm, G. Nyström, A. Mihranyan, M. Stromme, *Adv. Mater.* **2011**, *23*, 3751–3769.
[18] A. Ghosh, Y. H. Lee, *ChemSusChem* **2012**, *5*, 480–499.
[19] S. Bose, T. Kuila, A. K. Mishra, R. Rajasekar, N. H. Kim, J. H. Lee, *J. Mater. Chem.* **2012**, *22*, 767–784.
[20] S. Dutta, A. Bhaumik, K. C.-W. Wu, *Energy Environ. Sci.* **2014**, *7*, 3574–3592.
[21] S. Osman, R. A. Senthil, J. Pan, W. Li, *J. Power Sources* **2018**, *391*, 162–169.
[22] W. Xia, C. Qu, Z. Liang, B. Zhao, S. Dai, B. Qiu, Y. Jiao, Q. Zhang, X. Huang, W. Guo, *Nano Lett.* **2017**, *17*, 2788–2795.
[23] F. He, Z. Hu, K. Liu, S. Zhang, H. Liu, S. Sang, *J. Power Sources* **2014**, *267*, 188–196.
[24] D. T. Pham, T. H. Lee, D. H. Luong, F. Yao, A. Ghosh, V. T. Le, T. H. Kim, B. Li, J. Chang, Y. H. Lee, *ACS Nano* **2015**, *9*, 2018–2027.
[25] J. Deng, M. Li, Y. Wang, *Green Chem.* **2016**, *18*, 4824–4854.
[26] D. Wang, Z. Xu, Y. Lian, C. Ban, H. Zhang, *J. Colloid Interface Sci.* **2019**, *542*, 400–409.
[27] B. Zhu, K. Qiu, C. Shang, Z. Guo, *J. Mater. Chem. A* **2015**, *3*, 5212–5222.
[28] B. Zhu, C. Shang, Z. Guo, *ACS Sustainable Chem. Eng.* **2016**, *4*, 1050–1057.
[29] Q. Tian, X. Wang, X. Xu, M. Zhang, L. Wang, X. Zhao, Z. An, H. Yao, J. Gao, *Mater. Chem. Phys.* **2018**, *213*, 267–276.
[30] C. L. Ban, Z. Xu, D. Wang, Z. Liu, H. Zhang, *ACS Sustainable Chem. Eng.* **2019**, *7*, 10742–10750.
[31] L. Guan, L. Pan, T. Peng, C. Gao, W. Zhao, Z. Yang, H. Hu, M. Wu, *ACS Sustainable Chem. Eng.* **2019**, *7*, 8405–8412.
[32] X. Kang, H. Zhu, C. Wang, K. Sun, J. Yin, *J. Colloid Interface Sci.* **2018**, *509*, 369–383.
[33] C. Chang, H. Wang, Y. Zhang, S. Wang, X. Liu, L. Li, *ACS Sustainable Chem. Eng.* **2019**, *7*, 10763–10772.
[34] D. Qiu, C. Kang, A. Gao, Z. Xie, Y. Li, M. Li, F. Wang, R. Yang, *ACS Sustainable Chem. Eng.* **2019**, *7*, 14629–14638.
[35] K. Zou, Y. Deng, J. Chen, Y. Qian, Y. Yang, Y. Li, G. Chen, *J. Power Sources* **2018**, *378*, 579–588.
[36] L. Wan, P. Song, J. Liu, D. Chen, R. Xiao, Y. Zhang, J. Chen, M. Xie, C. Du, *J. Power Sources* **2019**, *438*, 227013.
[37] L. Wan, D. Chen, J. Liu, Y. Zhang, J. Chen, C. Du, M. Xie, *J. Alloys Compd.* **2020**, *823*, 153747.
[38] Y. Zhou, J. Ren, L. Xia, Q. Zheng, J. Liao, E. Long, F. Xie, C. Xu, D. Lin, *Electrochim. Acta* **2018**, *284*, 336–345.
[39] D. Kang, Q. Liu, J. Gu, Y. Su, W. Zhang, D. Zhang, *ACS Nano* **2015**, *9*, 11225–11233.
[40] C. Wang, D. Wu, H. Wang, Z. Gao, F. Xu, K. Jiang, *J. Mater. Chem. A* **2018**, *6*, 1244–1254.
[41] G. Zhao, Y. Li, G. Zhu, J. Shi, T. Lu, L. Pan, *ACS Sustainable Chem. Eng.* **2019**, *7*, 12052–12060.
[42] J. He, D. Zhang, Y. Wang, J. Zhang, B. Yang, H. Shi, K. Wang, Y. Wang, *Appl. Surf. Sci.* **2020**, *515*, 146020.
[43] M. E. Plonska-Brzezinska, D. M. Brus, A. Molina-Ontoria, L. Echegoyen, *RSC Adv.* **2013**, *3*, 25891–25901.
[44] Y. Gong, D. Li, C. Luo, Q. Fu, C. Pan, *Green Chem.* **2017**, *19*, 4132–4140.
[45] X. Su, S. Jiang, X. Zheng, X. Guan, P. Liu, Z. Peng, *Mater. Lett.* **2018**, *230*, 123–127.
[46] J. Liang, T. Qu, X. Kun, Y. Zhang, S. Chen, Y.-C. Cao, M. Xie, X. Guo, *Appl. Surf. Sci.* **2018**, *436*, 934–940.
[47] X. Bo, K. Xiang, Y. Zhang, Y. Shen, S. Chen, Y. Wang, M. Xie, X. Guo, *J. Energy Chem.* **2019**, *39*, 1–7.
[48] C. Zhao, Y. Huang, C. Zhao, X. Shao, Z. Zhu, *Electrochim. Acta* **2018**, *291*, 287–296.
[49] N. Cai, H. Cheng, H. Jin, H. Liu, P. Zhang, M. Wang, *J. Electroanal. Chem.* **2020**, *861*, 113933.
[50] F. Wu, J. Gao, X. Zhai, M. Xie, Y. Sun, H. Kang, Q. Tian, H. Qiu, *Carbon* **2019**, *147*, 242–251.
[51] M. Tianxiao, Z. Xiaoxue, W. Yanmei, *J. Energy Storage* **2019**, *26*, 101014.
[52] V. Yang, R. A. Senthil, J. Pan, A. Khan, S. Osman, L. Wang, W. Jiang, Y. Sun, *J. Electroanal. Chem.* **2019**, *855*, 113616.
[53] Y. Huang, J. He, Y. Luan, Y. Jiang, S. Guo, X. Zhang, C. Tian, B. Jiang, *RSC Adv.* **2017**, *7*, 10385–10390.
[54] M. A. Ahmad, R. Alrozi, *Chem. Eng. J.* **2010**, *165*, 883–890.
[55] N. Xiao, X. Zhang, C. Liu, Y. Wang, H. Li, J. Qiu, *Carbon* **2019**, *147*, 574–581.
[56] F. Zheng, Y. Yang, Q. Chen, *Nat. Commun.* **2014**, *5*, 5261.
[57] X. Lang, A. Hirata, T. Fujita, M. Chen, *Nat. Nanotechnol.* **2011**, *6*, 232–236.
[58] P. J. Kim, H. D. Fontecha, K. Kim, V. G. Pol, *ACS Appl. Mater. Interfaces* **2018**, *10*, 14827–14834.
[59] L.-F. Chen, X.-D. Zhang, H.-W. Liang, M. Kong, Q.-F. Guan, P. Chen, Z.-Y. Wu, S.-H. Yu, *ACS Nano* **2012**, *6*, 7092–7102.
[60] S. B. Kayiran, F. D. Lamari, D. Levesque, *J. Phys. Chem. B* **2004**, *108*, 15211–15215.
[61] K. Xiao, L.-X. Ding, H. Chen, S. Wang, X. Lu, H. Wang, *J. Mater. Chem. A* **2016**, *4*, 372–378.
[62] A. M. Stephan, T. P. Kumar, R. Ramesh, S. Thomas, S. K. Jeong, K. S. Nahm, *Mater. Sci. Eng. A* **2006**, *430*, 132–137.
[63] V. Subramanian, C. Luo, A. M. Stephan, K. Nahm, S. Thomas, B. Wei, *J. Phys. Chem. C* **2007**, *111*, 7527–7531.
[64] J. Han, G. Xu, B. Ding, J. Pan, H. Dou, D. R. MacFarlane, *J. Mater. Chem. A* **2014**, *2*, 5352–5357.
[65] Z. Li, Y. Jiang, L. Yuan, Z. Yi, C. Wu, Y. Liu, P. Strasser, Y. Huang, *ACS Nano* **2014**, *8*, 9295–9303.

Manuscript received: March 2, 2020
Revised manuscript received: April 1, 2020
Accepted manuscript online: April 16, 2020
Version of record online: May 5, 2020